

EXPERIMENTAL AND NUMERICAL MODEL INVESTIGATION OF VORTEX TUBE PERFORMANCE

Jiří LINHART¹, Richárd MATAS², Mohamed KALAL³

Abstract: An experimental study of the vortex tube has been carried out to investigate the effect of thermo-physical parameters. Experimental results of the temperature of the hot and cold air outlet of the vortex tube, with the cold air mass ratio (CAMR) and the pressure of the inlet air as parameters are presented. In this paper a computational fluid dynamics (CFD) package is used to investigate the performance and flow phenomena within a vortex tube. A three-dimensional CFD model has been developed that successfully exhibits all of the general behavior expected from a vortex tube.

1. INTRODUCTION

Vortex tube is a simple mechanical device operating as a refrigerating and heating machine with no moving parts. The vortex tube creates a helical vortex from compressed air and separates it into two air streams, one hot and one cold. Compressed air enters a cylindrical generator, which is proportionately of larger diameter than the long tube, where it causes the air to rotate. Then, the rotating air is forced to flow down along the inner wall of the tube at speeds reaching a sonic value. At the end of the hot tube, a small or big portion of this air exits through a needle valve (control valve) as the hot air exhaust. The remaining air is forced to flow back through the centre of the incoming air stream at a slower speed. The heat from the slower moving air is transferred to the faster moving incoming air, though here is a higher temperature. This cooled air flows rotationally along the generator centre line and exits the tube in the cold air exhaust port, as shown schematically in figure 1.

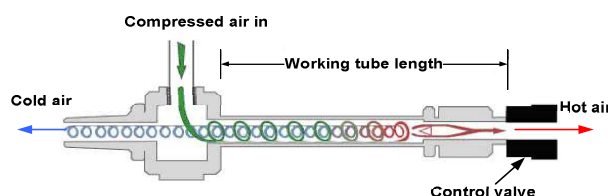


Fig. 1 Schematic diagram of a vortex tube

Ranque [1] was the earliest one who investigated compressed air flowing tangentially into a tube and found that air streaming near the wall had a higher temperature than that one near the axis. He tried to use this effect for refrigeration. Hilsch [2] as the first published systematical experimental results by varying the inlet pressure and the geometrical parameters of the tube. A recent review of the existing literature is given in [3]. In spite of the present uses and the various studies, no adequate physical explanation is available for the actual transport mechanism. Indeed, in the existing literature, there have been several, often contradictory, qualitative theories. Ahlborn, et al. [4] identified the temperature splitting phenomenon of a Ranque–Hilsch vortex tube in which a stream of gas divides itself into a hot and a cold flow as a natural heat pump mechanism, which is enabled by a secondary circulation. Ahlborn, et al. [5] considered the vortex tube as a refrigeration device which could be analyzed as a classical thermodynamic cycle, replete with significant temperature splitting, refrigerant, and coolant loops, expansion and compression branches, and natural heat exchangers.

¹ Jiří Linhart, prof., Ing, CSc, Department of Power System Engineering, Faculty of Mechanical Engineering, University of West Bohemia. Univerzitni 8, Plzen 306 14. Czech Republic. Tel.: +420 377 63 8132, Fax: +420 377 63 8102, E-mail: linhart@kke.zcu.cz

² New Technologies Research Centre, University of West Bohemia. E-mail: mata@ntc.zcu.cz

³ Department of Power System Engineering; Faculty of Mechanical Engineering, University of West Bohemia; E-mail: kalal@kke.zuc.cz

The effect of various parameters, such as nozzle area, cold orifice area, hot end area and L/D ratio of the tube length to the tube diameter, on the performance of the vortex tube was investigated in [6]. There were experimentally tested variations of the cold air temperature T_c with respect to the change of the hot end area for $L/D = 45, 50, 55$. Also the effects of length and diameter on the principal vortex tube are considered in [7]. They showed variation of efficiency versus different L/D of vortex tube. An experimental investigation of the energy separation process in the vortex tube was conducted in [8]. There were measured temperature profiles at different positions along the vortex tube axis with conclusion the vortex tube length has an important influence on the transport mechanism inside. In [9] there are presented experimental results of the energy separation in the vortex tube under different operating conditions showing the temperature changes of the cold and hot streams as a function of the inlet pressure. So far there are plenty of available researches validating the reliability of CFD analyses for the flow and temperature investigation within the vortex tube. Papers [10, 11] show the dependence of vortex tube performance on the normalized pressure drop by using a numerical model. [12] presents a numerical analysis in which the fluid dynamic equations are decoupled from the energy equation. The flow pattern was determined using the vortex stream function formulation of the radial and axial Navier-Stokes equation and a standard k- ϵ turbulence model. CFD can also be used as a minimal adequate tool for design of engineering components. [13] presents a detailed analysis of various parameters of the vortex tube through CFD techniques to simulate the phenomenon of flow pattern, thermal separation, pressure gradient etc. And also reveals its utility as a tool for optimal design of vortex tube towards the nozzle number optimization, nozzle profiles, cold end diameter, length to diameter ratio, cold and hot gas fractions. [6] showed successfully utilized a CFD model of the vortex tube to understand the fundamental processes that drive the power separation phenomena. CFD and experimental studies conducted towards the optimization of the Ranque–Hilsch vortex tubes are presented in [14]. They showed the swirl, axial and radial velocity components of the flow, and the flow pattern obtained through CFD. The optimum cold end diameter, the ratios of the vortex tube length to diameter and optimum parameters for acquiring the maximum hot gas temperature and minimum cold gas temperature are achieved by CFD analysis and validated through experiments

2. EXPERIMENTAL SETUP

The arrangement of experimental apparatus and measuring devices, which is used for the determination of the performance of the counter flow vortex tube, is shown in figure 2. The experimentation was started when the air was compressed by the air compressor (1). The high pressure air passes through the pressure tank (2) to suppress impacts and through the valve (3), where its mass rate is regulated. Inlet pressure is read by the pressure gage (4), and then goes through the dust filter (5) and cooler (6) with cyclone separator. The mass flow rate of the inlet air is measured using an orifice (7). Then the compressed air is introduced tangentially into the vortex tube (9), where it expands and separates into the hot and cold air streams. The cold air in the central region leaves the vortex tube near the entrance, while the hot air goes out to the surrounding at the far end of the vortex tube. The needle valve (10) controls the flow rate of the hot air. Just after the pipe, the mass flow rate of the hot air is measured using the orifice (12). Thermocouples numbered 8, 11 and 13 measure the inlet and outlet temperatures. All temperatures and pressures data were recorded with a data logger (14) on a PC (15). A program was written in Lab VIEW 7.2 to control the data logging parameters and to display the obtained results.

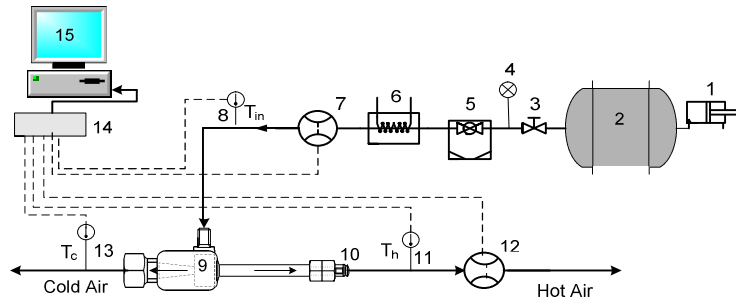


Fig. 2 Schematic diagram of the experimental setup

3. Experimental result

During the experimental test, the inlet pressure of the compressed air and the cold air mass ratio $CAMR = y$ were varied systemically. The CAMR is defined as follows:

$y = m_c/m_i$, where m_c represents the mass flow rate of the cold stream released, while m_i represents the inlet or total mass flow rate of the pressurized inlet working fluid. Therefore, the CAMR changes in the range $0 \leq \text{CAMR} \leq 1$. Tests have been conducted at inlet pressure of 2.7, 4, 6 and 8 bars, at constant inlet temperature 20°C . The experimental temperatures and temperature differences of hot and cold outlet air are shown in Figure 3, as a function of the cold air mass ratio.

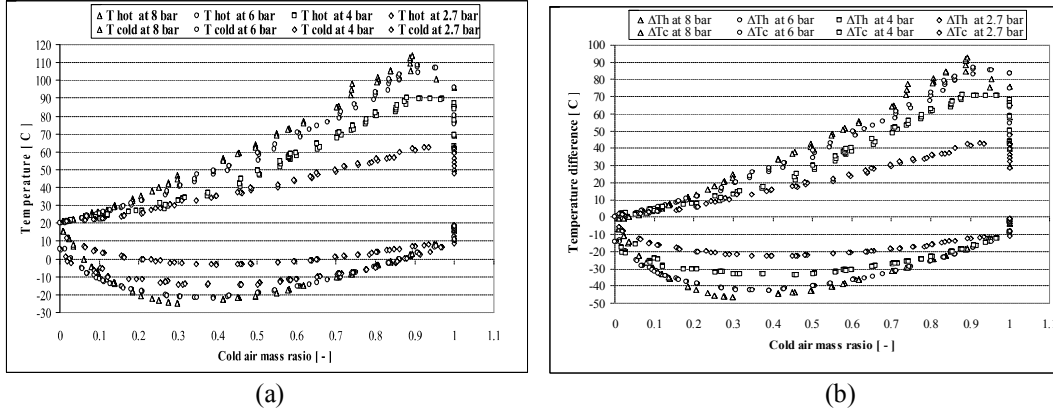


Fig. 3 Hot and cold temperatures (a), hot and cold temperature differences (b) as a function of cold mass ratio

All tests were run at first by holding a constant inlet temperature. Obviously, it can be seen that the temperature of the hot exit air increases with raising CAMR from null up to nearly 0.9. With further increase of the cold air mass ratio higher than 0.85 the hot exit air temperature achieves a maximum value and then decreases to its minimum one. The range of the CAMR, at which the hot outlet air becomes a maximum, is from 0.85 to 0.90. At the cold air mass ratio from 0.9 up to 1 a sharp temperature drop is measured for the hot air exit temperature. It is evident that the figure 3(a) can be divided into three parts according to the parameter CAMR: 0-0.4, 0.4-0.9, and 0.9-1. In the main central region of the diagram act three mechanisms determining state and development of the flow in tube.

In the vicinity of the wall prevails molecular friction caused by the high velocity decrement at the wall and in the boundary between the hot flow and the back cold flow. This is source of heating of the main flow streaming along the wall to the hot exit. Besides here acts further mechanism, probably the most important, namely separation of rapid (hot) and slow (cold) molecules. The molecules of high velocity are centrifuged to the margin layer of the tube cross section and strongly contribute to the higher temperature of the hot flow. The slow molecules are attracted to the tube centre because there is a lower pressure induced by the swirl flow in the tube. This molecular diffusion orientated from outside to the centre contributes to the low temperature in the central cold flow. The mentioned mechanism stops acting in the CAMR region from 0 to 0.4. The reason is small mass flow rate of the cold flow at which the regular flow pattern is violated and diffusion including centrifuging process interrupted. At this situation exist in vicinity of the cold outlet orifice two flows, one going out and the other into the tube. For the third CAMR region is characteristic the inside flow not achieving the hot end of the tube and the separation model of molecules is dislocated again. In all the measured cases the temperature of the exit hot air is higher than that of the inlet air, $T_h > 20^\circ\text{C}$. Figure 3 gives also the temperature and temperature difference of outlet air as a function of the inlet pressure as a parameter. It can be seen that the temperature of the hot outlet increases with inlet pressure increasing, and that the cold outlet temperature decreases with inlet pressure.

The temperature differences between the hot outlet air and the inlet air, $\Delta T_h = T_h - T_i$, and between the cold outlet air and the inlet air, $\Delta T_c = T_c - T_i$, as functions of the CAMR, with the pressure of the inlet air as a parameter are presented in figure 3(b). With the outflow of the hot air coming near zero, $y = 1$, the temperature of the gas at the hot air outlet is higher than that of the inlet air. Similarly without the outflow of the cold air, $y = 0$, the temperature measured at the outlet of the cold air, is lower than the temperature of the inlet air. Also Figure 3(b) demonstrates that for CAMR in a range from 0.1 to 0.4, there is distinctively a potential of higher rate of temperature reduction in the cold outlet but lower rate of temperature reduction for the range around 0.4. For the CAMR in a range between 0.3 and 0.4, there is the lowest temperature reduction in the cold outlet for all inlet pressures supplied. When inlet pressures are at 2.7, 4, 6 and 8 bars, the corresponding highest temperature drops in the cold outlet are 22°C , 33°C , 42°C and 46°C respectively. The higher is the inlet pressure the more decreasing temperature is obtained for each CAMR used.

4. CFD MODEL

The CFD system FLUENT in version 6.1 was used for the vortex tube numerical simulations. The numerical model was based on experiences with previous solved axisymmetric models [15]. Geometry of the vortex tube simulated by a 3D CFD model is depicted in figure 4. The length is 92mm and inside diameter 5.2mm. The geometry comes from the simultaneously measured vortex tube and is simplified. Its periodical segment (angle 60°) was used for the simpler solving; the hot outlet valve wasn't simulated completely and the control valve was replaced by the pressure outlet with variable area.

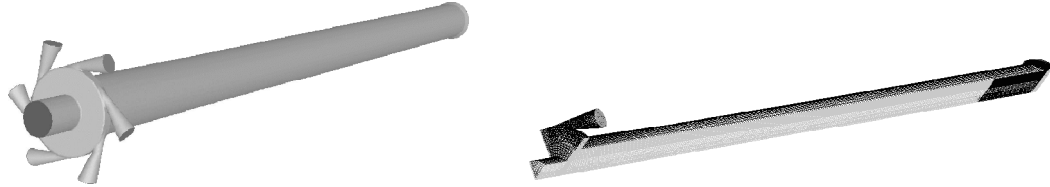


Fig.4 Geometry of the CFD model and computational mesh of the solved periodical segment

5. CFD COMPUTATION

Computational mesh of the periodical segment has about 70 000 mixed cells. The parameters of the model were set up following: inlet mass flow rate 6.10^{-4} kg/s (one inlet nozzle), inlet total temperature 20 °C, outlet pressure 95 600 Pa, the walls were regarded as adiabatic. It is necessary to initialise the computation suitably in order to obtain converging solution. The computations converged relatively slowly, the number of iterations leading to a converged solution was more than 10 000. The standard k-ε model was used, the relation between turbulent and laminar viscosity was reduced to 500 to obtain more realistic velocity profiles, see [15]. The inlet turbulent intensity in described model was set to 3 %. The turbulent Prandtl number in the turbulent model was substantially increased because the performed simulations have given the best results for $Pr_t = 9$. Computed results were satisfactory. The computed inlet total pressure for the given mass flow rate was 7.10^5 Pa. This value is the same as measured in experiment. Figure 5 shows radial – axial velocity field in the vortex tube for the CAMR 0.5183. It is possible to see the basic character of the flow field, which corresponds to the flow field described by other authors.



Fig. 5 Velocity vectors without tangential component in various locations of the vortex tube for the cold fraction 0.5183

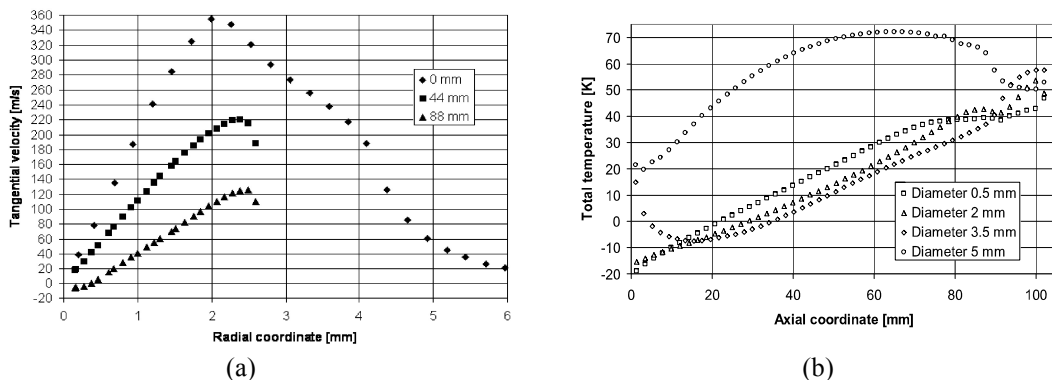


Fig.6. (a) Tangential velocity profiles in the slice 0, 44 and 88 mm from the plane of the inlet nozzles for the cold fraction 0.5183; (b) Total temperature profiles on the diameters 0.5, 2, 3.5 and 5 mm for the cold fraction 0.5183

Figure 6(a) shows the tangential velocity profiles in the slice 0.0, 44 and 88 mm ($x/D=0.44, 0.90$) from the plane of the inlet nozzles. There is evident decrease of the tangential velocity from the inlet and cold outlet to the hot outlet. The total temperature distribution shows figure 6(b). It is noticeable that the increase of the total temperature from inlet to the hot outlet is relatively constant in the diameter 3.5 mm and the own increase of the temperature occurs in the relatively thin layer adjacent to the wall of the vortex tube.

In figure 7 you can see the distribution of the total temperature in the tube for various CAMR. The behaviour of the tube is changed in the range 0.63 to 0.79 of the CAMR, where the temperature distribution has a different order.

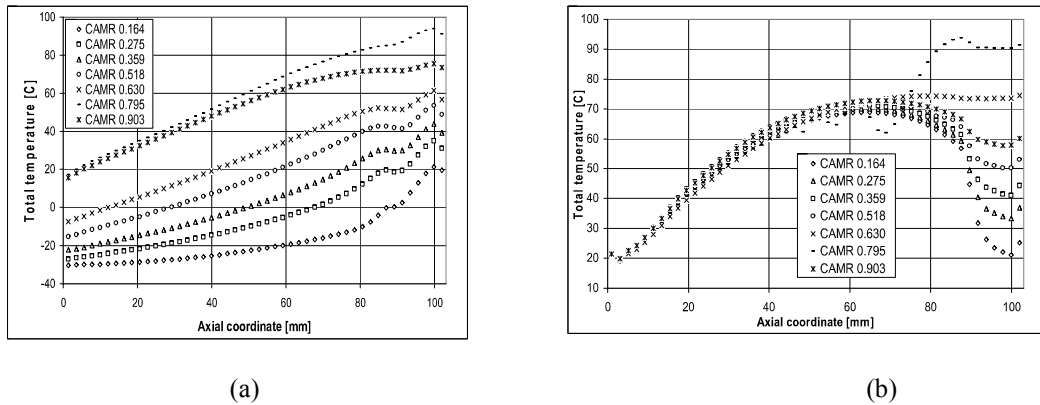


Fig.7. Total temperature profiles for the various cold fractions: (a) for the diameter 2 mm (up) , (b) 5 mm (down)

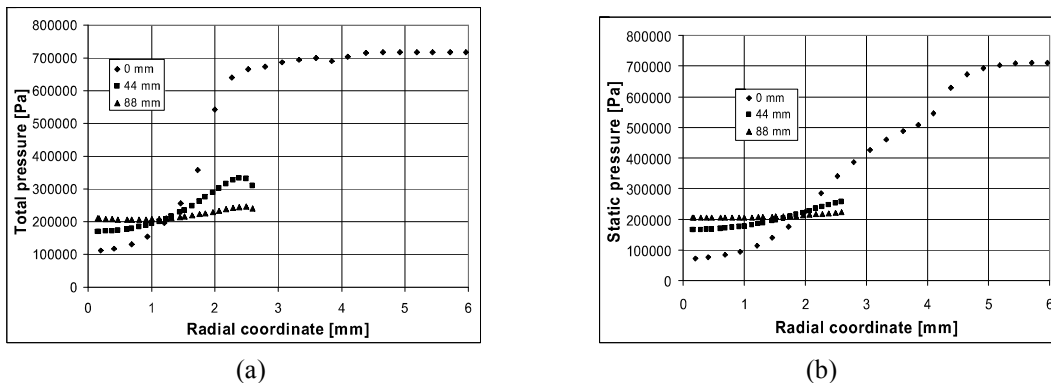


Fig.8. Pressure profiles in the slice 0, 44 and 88 mm from the plane of the inlet nozzles for the cold fraction 0.5183: (a) for Total pressure, (b) Static pressure

Figures 8 represent the total and static pressure in the slices 0.0, 44 and 88 mm from the plane of the inlet nozzles. We see the minimum pressure in centre of the vortex tube that is caused by the rotation movement of the air. At the wall, the pressure sinks in direction of the hot exit and in the centre has an opposite gradient. Both the pressure courses are closely linked with correct function of the tube.

6. COMPARISON OF EXPERIMENT AND CFD SIMULATION

The inlet temperature and inlet mass flow rate in the CFD model were specified as a constant 20°C and 0.0036 kg/s respectively, which is consistent with the measured total temperature at the inlet to the vortex tube. The results of the experimental model were compared with three-dimensional, axisymmetric CFD models that were developed using the commercial CFD code FLUENT. Figure 9 shows the experimental and CFD analysis of the hot and cold temperature of air as a function of the parameter CAMR. It can be seen that maximum hot outlet temperature of 90.8°C (at 0.8 of CAMR) is obtained from CFD analysis and about 112°C (at 0.89 of CAMR) is obtained from experiments. And a minimum cold outlet temperature of -22.6°C (at 0.36 of CAMR) is obtained from CFD analysis and about -24.6°C (at 0.35) of CAMR) is obtained from experiments. Thus CFD analysis is in acceptable agreement with experimental results if we realize the number of approximations that are necessary to do in the simulation.

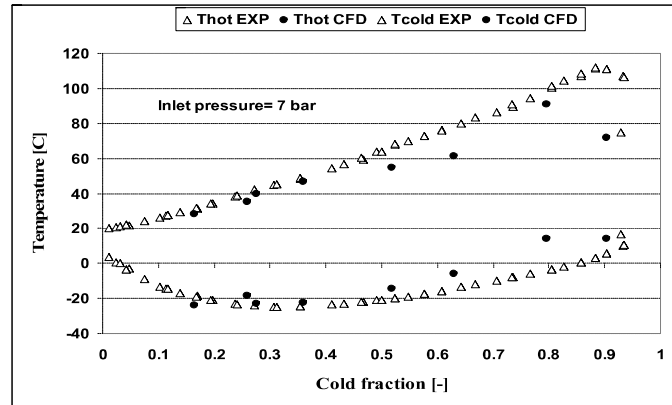


Fig.9. Experimental and CFD analysis of the hot and cold air temperature as a function of CAMR.

7. CONCLUSIONS

Experimental results of the hot and cold air outlet temperatures of the vortex tube, with the dimensionless cold air flow rate CAMR and the inlet air pressure as parameters are presented. It is clear from our experiments that the CAMR is an important factor affecting the vortex tube performance.

The CFD study has shown that numerical computation of the vortex tube is possible if a convenient model is chosen and special computing parameters set up (turbulent Prandtl number). The computation offers inside flow values - velocity, static and total temperature, static and total pressure profiles - that cannot be obtained by a simple measurement.

REFERENCES

- [1] Ranque GJ, 1933, "Experiences sure la détente giratoire avec productions simultanees d'un echappement d'air chaud et d'un echappement d'air froid", *J Phys Radium*, Vol.4, pp. 112-4.
- [2] Hilsch R, 1947, "The use of the expansion of gases in a centrifugal field as a cooling process", *Rev Sci Instrum*, Vol. 8, pp.108-13.
- [3] Cocerill T, 1998, "Thermodynamics and Fluid Mechanics of a Ranque-Hilsch Vortex Tube", Ph. D. Thesis, University of Cambridge.
- [4] Ahlborn B, Keller JU, Rebhan E, 1998, "The Heat Pump in a Vortex Tube" *J Non- Equilib Thermodyn*, Vol. 23(2), pp. 159-65.
- [5] Ahlborn BK, Gordon JM, 2000, "The Vortex Tube as a Classical Thermodynamic Refrigeration Cycle", *J Appl Phys*, Vol.88 (6), pp.3645-53.
- [6] N.F. Aljuwayhel, G.F. Nellis, S.A. Klein, 2005, "Parametric and Internal Study of the Vortex Tube using a CFD model", *Int J Refrigeration* Vol. 28 (3), pp. 442-450.
- [7] Saidi M H and Valipour M S, 2003, "Experimental modelling of vortex tube refrigerator". *Applied thermal engineering*. Vol. 23, No. 15 pp 1971-1980.
- [8] Stephan K, Lin S, Durst M, Hunag F and Seher D, 1983, "An investigation of Energy Separation in a Vortex Tube", *International Journal of Heat and Mass Transfer*, Vol. 26, No.3, pp 341-388.
- [9] Ting-Quan MA, Qing-Guo, Jian YU, Fang YE, and Chong-Fang, 2002, "Experimental investigation on energy separation by vortex tubes". *12th international Heat Transfer Conference*, 10, Paris.
- [10] H.H. Bruun, 1969, "Experimental Investigation of the Energy Separation in Vortex Tubes", *J Mech Eng Sci*, Vol. 11 (6), pp. 567-582.
- [11] B. Ahlborn, J.U. Keller, R. Staudt, G. Treitz, R. Rebhan, 1994, "Limits of Temperature Separation in a Vortex Tube", *J Phys D: Appl Phys* 27, pp. 480-488.
- [12] B.Ahlborn, J. Camire, J.U. Keller, 1996, "Low-Pressure Vortex Tubes", *J Phys D: Appl Phys*, Vol. 29, pp.1469-1472.
- [13] W. Frohlingdorf, H. Unger, 1999, "Numerical Investigations of the Compressible Flow and the Energy Separation in Ranque-Hilsch Vortex Tube", *Int. J. Heat Mass Transfer*, Vol. 42, pp.415-422.
- [14] Upendra Behera, P.J. Paul, S. Kasthuriangan, R. Karunanithi, S.N. Ram, K. Dinesh and S. Jacob, 2005, "CFD analysis and experimental investigations towards optimizing the parameters of Ranque-Hilsch vortex tube", *Int. J. Heat and Mass Transfer*, Vol. 48, Issue 10, 2005. pp. 1961-1973
- [15] Jiří Linhart, Mohamed Kalal, Richard Matas, 2005, "Numerical study of vortex tube properties", *16th international symposium on transport phenomena*, Prague, Czech Rep.